Bulletin of the Seismological Society of America, 92, 1, pp. 194–207, February 2002

Postseismic Deformation near the İzmit Earthquake (17 August 1999, *M* 7.5) Rupture Zone

by S. Ergintav, R. Bürgmann, S. McClusky, R. Çakmak, R. E. Reilinger, O. Lenk, A. Barka, and H. Özener

Abstract We present and interpret the results of postseismic, Global Positioning System monitoring of the first 298 days following the 17 August 1999 İzmit earthquake. Whereas the data suggest some spatial and temporal complexity in the postseismic motions, the overall pattern can be characterized by time-dependent relaxation functions and suggests exponential decay with an estimated 57-day relaxation time. The very rapid deformation during the first few weeks following the mainshock suggests rapid afterslip on and below the coseismic rupture segments. The exponential decay of the postseismic deformations through the end of the observation period suggests contributions from the lower crustal viscoelastic relaxation.

Introduction

Major earthquakes are important keys to understanding crustal deformation phenomena, including coseismic (main rupture and early aftershocks) and postseismic effects (including a short-term afterslip phase and a long-term viscoelastic relaxation phase) (e.g., Pollitz *et al.,* 1998). Whereas the distribution of the coseismic fault slip provides valuable information about the mechanics of the earthquake process on the main fault zone, the postseismic deformation provides clues about the mechanical behavior of the region surrounding the coseismic fault and in deeper parts of the earthquake generation zone (Savage, 1980; Thatcher, 1983; Tse and Rice, 1986; Scholz, 1988). Knowledge of the distribution of coseismic and postseismic deformation and associated stress changes can also improve estimates of seismic hazard on neighboring faults.

In addition to the spatial pattern of surface displacements, the temporal development of postseismic deformation provides clues about the rheology of the fault zone and the surrounding crust. The distribution of the afterslip characterizes time-dependent stressing following earthquakes and directly reflects the material properties of the fault zone. Improved knowledge of the longer term relaxation process may lead to a means of distinguishing between power law and linear viscoelastic flow in the lower crust and upper mantle and is important for the long-term transfer of stress across fault zones in response to crustal stress release (Chen and Molnar, 1983; Pollitz *et al.,* 1998). The separation of the afterslip and viscoelastic relaxation mechanisms can be difficult, and, as is the case for long strike-slip faults, the two types of models predict very similar surface deformation (Savage and Prescott, 1978; Thatcher, 1983; Savage, 1990). Nonetheless, improved understanding of the timescale and spatial scale of postseismic deformation has implications for crust and mantle rheology and the mechanical properties of fault zones.

The most recent large events to occur along the North Anatolian Fault (NAF) zone, the İzmit and Düzce earthquakes (17 August 1999, M_w 7.5 and 12 November 1999, M_w 7.1), thus provide the opportunity to significantly improve our understanding of the mechanical behavior of the NAF, the response of the crust to coseismic stress changes, and the future seismic risk in western Turkey.

Following the İzmit and Düzce earthquakes, a large Global Positioning System (GPS) data set was collected, including contributions from the Marmara Continuous Global Positioning System Network (MAGNET), additional continuous GPS stations installed by The Scientific and Technical Research Council of Turkey (TÜBİTAK), Earth and Marine Sciences Research Institute (EMSRI), and repeated GPS surveys of many bench marks in the area. These continuous and campaign-style survey sites provide detailed information about the temporal and spatial patterns of postseismic deformation.

In this article, we describe and characterize the temporal and spatial behavior of postearthquake transient deformation during the first 298 days following the İzmit earthquake. We evaluate different parameterizations of relaxation functions constrained by the GPS time series, which characterize the temporal character of the postseismic relaxation. Based on the form of the relaxation function, we discuss possible implications for the mechanical properties of the upper crust and the viscoelastic response of the lower crust and upper mantle. The GPS time series also reveal deformation associated with a large M_w 5.9 aftershock that we model in terms of slip on the coseismic fault. Whereas we focus in this study on the general attributes of postseismic relaxation and de-

termine the total cumulative displacements during the first 298 postseismic days, a related article (Bürgmann *et al.,* 2002) presents spatially and temporally variable afterslip models based on the same GPS data, up to the time of the 12 November Düzce earthquake.

GPS Measurements

Because the Marmara Sea region had been identified as a seismic gap likely to generate large earthquakes (Toksöz *et al.,* 1979), the MAGNET (Yalçin *et al.,* 1999; *www.ydbae.mam.gov.tr*) was established before the İzmit earthquake to measure the deformation associated with strain accumulation along the western NAF system (Fig. 1). Five continuous GPS stations of MAGNET (TUBI, DUMT, MERT, KANT, MADT) were operating before the İzmit earthquake within the coseismic rupture zone. Four additional continuously recording GPS stations were installed by TÜBİTAK, EMSRI, within 48 hr of the mainshock in order to track early transient postseismic deformation. Two of them (UCGT, BEST) were located approximately 15 km north of the fault break, and two others (HAMT, MURT) were installed less than 10 km south of the rupture. Two weeks later, another station (ULUT) was installed approximately 80 km from the rupture zone in the southern part of the İzmit rupture area to track far-field deformation. Existing GPS monuments (62 sites) were occupied within 1 week following the İzmit earthquake (measurement periods >10 hr) in order to constrain the coseismic slip (Reilinger *et al.,* 2000), and a selected subset (36) was reoccupied multiple times. These sites were distributed along the fault break and extend out to 70 km from the surface break. Additional sites are located up to 200 km from the rupture and were observed on a less frequent basis. Following the Düzce earthquake, two additional continuous GPS stations (ABAT and YIGT) were installed near the Düzce rupture within 24 hr of the event. Their locations are approximately 30 km south and north of the Düzce rupture, respectively (Fig. 1).

Whereas MAGNET stations have good quality pillars, the antennas of all semicontinuous stations (BEST, UCGT, MURT, HAMT, YIGT, ABAT) were mounted on tripods for rapid postearthquake deployment. During the 11-month observation time, all semicontinuous stations were periodically visited to control the antenna centering and height. This was an important task because of the low signal-to-noise-ratio of the nonlinear postseismic displacements. Nonetheless, the measurements at these stations were noisier than MAGNET stations because of the bigger seasonal variations of the marker, antenna setup problems, and vandalism.

Figure 1 shows the network configuration, the trace of the surface breaks of the İzmit and Düzce earthquakes, and known active faults in the region. In addition to the mapped trace of the İzmit coseismic surface rupture segments, the figure includes the Yalova fault segment to the west of the Hersek delta, which likely experienced only a small amount of coseismic slip along its eastern edge ($\sim$15 km) (Reilinger *et al.,* 2000). The MAGNET stations, the semicontinuous stations of TÜBİTAK, EMSRI, and repeated survey sites are marked with different symbols in Figure 1 in order to show the differences in marker quality and occupation time. The occupation history of individual GPS sites is listed in Table 1.

Time-Dependent Motions from GPS Measurements

The GPS data were processed following standard procedures using the GAMIT/GLOBK GPS processing software (Herring, 2000; King and Bock, 1998). At first, doubly differenced GPS phase observations from each day were used to estimate station coordinates, the zenith delay and the gradients of the atmosphere at each station, and orbital and Earth orientation parameters (EOPs) by applying loose *a priori* constrains to all parameters. A reliable set of International GPS Service (IGS) stations was included within the analysis to establish a link between regional and global networks. In the second step, the loosely constrained estimates of station coordinates, orbits, EOPs, and their covariance from each day were used as quasi-observations in a Kalman filter to estimate a consistent set of daily coordinates. In this step, we combined for each day the quasi-observations from our regional analysis with the quasi-observations of a global analysis of IGS data performed by Scripps Orbit and Permanent Array Center. The reference frame was constrained on each day using a reliable set of global IGS stations. Positions of the fiducial IGS stations were constrained to ITRF97 coordinates. Further details about the processing method are described by McClusky *et al.* (2000).

We show the time series for the north and east components of station BEST in Figure 2. The error bars of the daily solutions indicate one standard deviation. The unadjusted time series (Fig. 2, top) has a significant coseismic jump on 12 November 1999 because of the Düzce earthquake and also shows the effects of displacement transients and aftershocks (e.g., 13 September 1999, M_L 6.2, M_w 5.9). In order to reduce the effects of aftershocks and the Düzce earthquake on the time series of the postseismic displacements, we removed offsets caused by the Düzce earthquake using a detailed coseismic model (Ayhan *et al.,* 2001). We did not attempt to remove the postseismic signature of the Düzce earthquake, but when computing the parameters of a common relaxation function, we omitted the heavily effected sites that experienced transient postseismic motions caused by the Düzce earthquake. Some additional outliers were also removed from the time series. The edited versions of the BEST time series are shown in Figure 2 (bottom). We show the edited versions of all available time series that were obtained during the 298-day observation period in Figure 3.

In Figure 3, daily GPS solutions are constrained to a Eurasia-fixed reference frame by minimizing the velocities

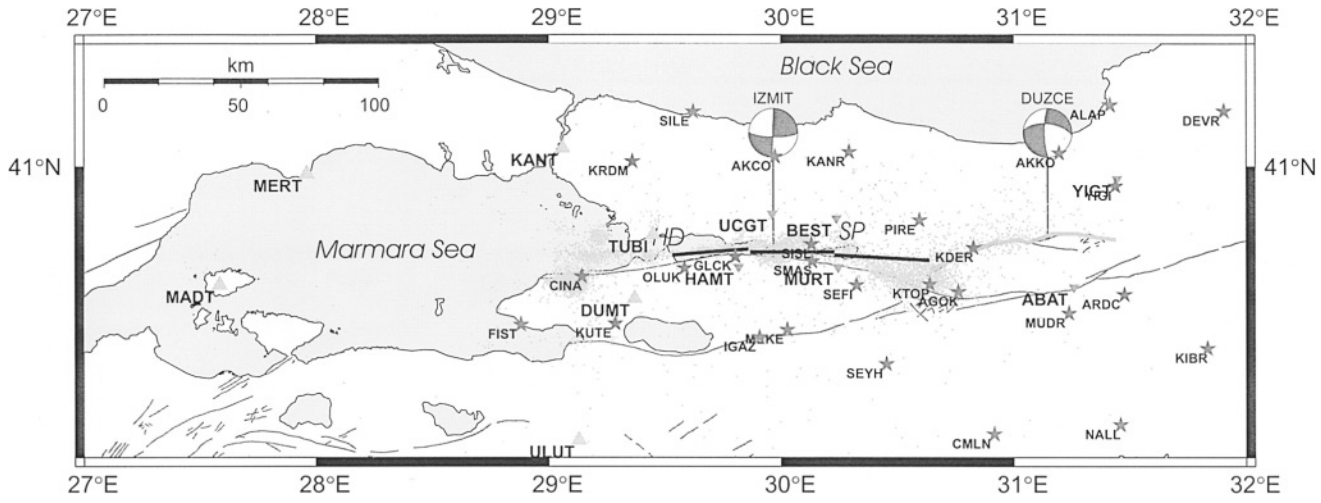

Figure 1. Map of the İzmit region showing MAGNET stations (▲), semicontinuous GPS stations (▼), and campaign sites (⋆). Heavy segmented lines indicate the fault ruptures of the Izmit earthquake, and gray-segmented lines indicate the fault ruptures of the Düzce earthquake (Reilinger *et al.,* 2000). The fault plane solutions of these events are also displayed and the aftershocks (until 10 October 1999) are shown as gray dots (Özalaybey *et al.,* 2001). Thin lines show the trace of active faults (Barka, 1997). (HD, Hersek Delta; SP, Sapanca).

of 13 global IGS stations in Europe (McClusky *et al.,* 2000). Each time series shows a somewhat different temporal behavior depending on the distance from the fault zone. Whereas near-field sites show an exponential decay (e.g., UCGT, MURT), far-field sites indicate more linear behavior (e.g., MADT, MERT). Some sites show short-period deformations, which may be caused by surficial, nontectonic processes. For example, the apparent periodic motion of HAMT may be because of such causes.

To better understand the effects of aftershocks on the time series, we analyzed the GPS data from continuous sites in 6-hr sessions. We modeled the site motions associated with the biggest aftershock (13 September 1999, M_L 6.2, M_w 5.9) using rectangular dislocations in an elastic, homogeneous, and isotropic half-space (Okada, 1985). To estimate the fault geometry, we used a constrained, nonlinear optimization algorithm (Bürgmann *et al.,* 1997). As can be seen in Figure 4, our estimates may not be well constrained because of insufficient data coverage. However, our model fault plane lies near the epicenter, is roughly coincident with the coseismic fault, and is characterized by predominantly right-lateral slip (consistent with the focal mechanism). Furthermore, our geodetic moment estimate is comparable to that of the seismic moment tensor (geodetic moment magnitude, $\mathbf{M}_w$ 5.95). Individual smaller aftershocks do not lead to significant site motions that can be resolved by the data. Comparisons of the total moment release from aftershocks and the geodetic moments determined from afterslip models indicate that the transient surface displacements are mostly caused by aseismic processes rather than deformation from aftershocks (Reilinger *et al.,* 2000).

Estimating Decay Constants and Cumulative Site Displacements

Neglecting nonlinear site motions, Reilinger *et al.* (2000) computed linear postseismic displacement rates in a weighted least-squares procedure from the station coordinates of the 75-day solutions and their covariance. However, the new observations covering 298 days clearly show that the temporal and spatial postseismic deformation rates changed with time. Accordingly, we estimate the time-dependent relaxation function for each site. We assume that the time series reflect a common relaxation process that describes the rheological behavior of the medium or fault zone, and we estimate a common relaxation function and relaxation time using all time series. This allows us to estimate the temporal behavior of the postseismic deformation using a simplified functional form.

The general form of the time (t)-dependent relaxation function can be defined as

$$\varepsilon = \varepsilon_0 + DR(t,\tau) + \dot{\varepsilon}t,$$

where ε_0 is the station position directly after the earthquake and D is the amplitude of the relaxation that constrains the rheological properties of the relaxing medium (Ranalli, 1987). $R(t, \tau)$ describes the functional form of the relaxation process, such as logarithmic, exponential, or power-law, and τ is the relaxation time constant or relaxation time. The last term $\dot{\varepsilon}$ represents a linear secular velocity.

A transient deformation stage, where strain increases with time at a decreasing rate, occurs following the instan-

Table 1

Station List, Their Occupation Histories, and Estimated Cumulative Station Displacements with 1-Sigma Uncertainties for the First 298 Days following the Izmit Earthquake

Site	Latitude (°)	Longitude (°)	First	Last	Duration (yr)	#	Descriptions	North (mm)	East (mm)	Uncertainties North (mm)	Uncertainties East (mm)
ABAT	40.6037	31.2593	1999.87	2000.42	0.55	183	MAGNET*	–	–	–	–
AGOK	40.5889	30.7611	1999.65	2000.37	0.72	10	Campaign	−0.9	−61.5	20.1	33.9
AKCO	41.0335	29.9731	1999.66	2000.24	0.57	4	Campaign	−10.4	50.7	111.5	145.9
AKKO	41.0446	31.1979	1999.67	2000.23	0.56	4	Campaign	18.3	28.8	26.2	43.1
ALAP	41.2006	31.4168	1999.82	2000.23	0.41	3	Campaign	–	–	–	–
ARDC	40.5798	31.4785	1999.66	2000.36	0.70	4	Campaign	31.9	−33.0	21.7	37.7
BEST	40.8291	30.2387	1999.63	2000.44	0.80	280	MAGNET*	−16.5	92.8	2.7	3.9
CINA	40.6395	29.1431	1999.65	2000.23	0.58	5	Campaign	−16.3	−33.0	26.2	37.8
CMLN	40.1179	30.9164	1999.66	2000.23	0.57	4	Campaign	0.7	−33.6	30.6	53.5
DUMT	40.5655	29.3719	1999.63	2000.24	0.82	270	MAGNET	−22.3	−50.5	2.1	3.3
FIST	40.4806	28.8818	1999.66	2000.23	0.56	5	Campaign	−4.6	−37.2	37.6	47.9
GLCK	40.7052	29.8038	1999.65	2000.24	0.59	6	Campaign	−17.1	−22.9	26.9	38.2
HAMT	40.6701	29.8187	1999.64	2000.45	0.81	289	MAGNET*	−47.6	−32.0	2.7	4.0
IGAZ	40.4380	29.9080	1999.67	2000.23	0.56	6	Campaign	−29.6	−70.9	28.4	39.7
KANR	41.0483	30.2936	1999.66	2000.23	0.57	6	Campaign	33.2	37.7	23.2	36.1
KANT	41.0608	29.0614	1999.63	2000.45	0.82	298	MAGNET	−22.5	11.3	2.3	3.4
KDER	40.7348	30.8266	1999.65	2000.23	0.57	8	Campaign	15.3	−41.0	34.0	70.5
KIBR	40.4003	31.8345	1999.83	2000.24	0.42	3	Campaign	–	–	–	–
KRDM	41.0171	29.3625	1999.67	2000.23	0.58	3	Campaign	−27.6	29.1	30.5	42.6
KTOP	40.6143	30.6381	1999.65	2000.23	0.57	10	Campaign	−1.7	−76.5	30.3	58.1
KUTE	40.4847	29.2879	1999.66	1999.88	0.57	3	Campaign	−29.6	−43.7	50.2	79.8
MADT	40.6114	27.5869	1999.63	2000.25	0.62	159	MAGNET	−4.6	−14.4	3.6	5.7
MEKE	40.4647	30.0264	1999.66	2000.25	0.60	5	Campaign	−18.7	−73.6	24.7	34.5
MERT	40.9669	27.9617	1999.63	2000.42	0.79	206	MAGNET	−5.4	−6.2	2.5	4.0
MHGZ	40.0279	30.5704	1999.66	2000.23	0.57	4	Campaign	10.9	−47.4	34.2	66.8
MUDR	40.5173	31.2398	1999.67	2000.24	0.58	6	Campaign	−11.9	−60.4	22.2	33.6
MURT	40.6697	30.2453	1999.63	2000.45	0.82	290	MAGNET*	−13.5	−81.4	2.6	3.9
NALL	40.1482	31.4598	1999.83	2000.25	0.42	3	Campaign	–	–	–	–
OLUK	40.6671	29.5853	1999.65	2000.25	0.60	5	Campaign	−14.8	−48.9	44.5	60.5
PIRE	40.8243	30.5952	1999.66	2000.23	0.57	7	Campaign	−2.2	86.9	22.1	34.7
SEFI	40.6116	30.3252	1999.65	2000.23	0.58	5	Campaign	10.6	−94.2	31.1	50.5
SEYH	40.3506	30.4534	1999.82	2000.25	0.44	3	Campaign	3.6	−40.9	124.4	181.0
SILE	41.1795	29.6232	1999.67	2000.25	0.57	3	Campaign	−33.2	24.7	28.2	39.9
SISL	40.7453	30.1303	1999.65	2000.24	0.59	6	Campaign	11.9	64.7	33.5	47.1
SMAS	40.6897	30.1340	1999.65	2000.24	0.59	6	Campaign	9.4	−72.8	35.3	50.6
TUBI	40.7867	29.4507	1999.63	2000.45	0.82	285	MAGNET	−16.7	26.2	2.4	3.5
UCOT	40.8457	29.9623	1999.63	2000.27	0.65	222	MAGNET*	−31.9	24.4	3.4	5.1
ULUT	40.0975	29.1314	1999.72	2000.29	0.57	126	MAGNET*	−9.8	−35.7	6.3	9.4
YIGI	40.9370	31.4388	1999.67	2000.24	0.57	11	Campaign	0.5	31.7	24.5	42.3
YIGT	40.9591	31.4464	1999.87	2000.03	0.17	61	MAGNET*	–	–	–	–

1-sigma uncertainties plotted with 95% confidence ellipses in Figure 7.
The blank cells indicate sites that were not included because of the effects of the Düzce earthquake.
*Continuous sites installed after the Izmit earthquake.

taneous deformation during the earthquake. Transient deformation is followed by a return to steady-state deformation ($\dot{\varepsilon}$), where the strain rate is a constant after some time determined by τ. The relaxation amplitudes depend on the rheology of the crust and upper mantle, and on the local conditions around the site (i.e., unconsolidated sediments and crustal heterogeneity). In other words, D is a function of the stress release in the medium and reflects the response of the medium after the earthquake.

Whereas power-law relaxation is often related to the decay of aftershock seismicity and the continuous rupture mechanism, logarithmic relaxation is commonly attributed to decaying afterslip (Marone *et al.,* 1991) and exponential relaxation could be related to viscoelastic processes (Shen *et al.,* 1994; Savage and Svarc, 1997). The form of the logarithmic ($R_l(t, \tau)$), the exponential ($R_e(t, \tau)$), and the power-law ($R_p(t, \tau)$) relaxation can be given as

$$R_l(t,\tau) = \log(1 + (t - t_{eq})/\tau),$$
$$R_e(t,\tau) = 1 - \exp(-(t - t_{eq})/\tau),$$
$$R_p(t,\tau) = ((t - t_{eq})/\tau)^{1-p},$$

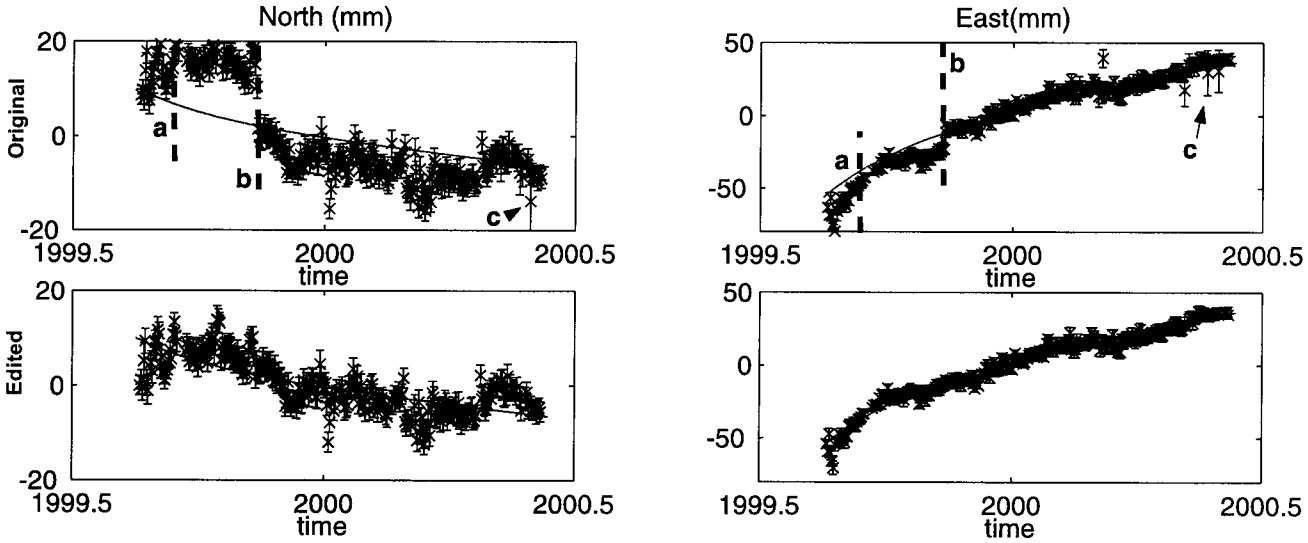

Figure 2. Top: Time series of north and east coordinates of station BEST. Bottom: Edited time series corrected for offsets from the largest aftershock and the Düzce earthquake. (a) The time of the biggest aftershock (13 September 1999). (b) The time of the Düzce earthquake (12 November 1999). (c) Noisy daily GPS solutions.

where t_{eq} is the time of the earthquake and p is the power-law index.

To obtain the best-fit common relaxation function for the time series, we selected 35 sites with a sufficient number of occupations to clearly show the postseismic relaxation. We removed two continuous sites (ABAT and YIGT) because they were installed after the Düzce earthquake and include large Düzce postseismic deformations. Some campaign sites (NALL, KIBR, ALAP) were also excluded because these sites are very near the rupture zone of the Düzce earthquake and are affected by Düzce postseismic motions. All unknown parameters (ε_0, $\dot{\varepsilon}$, D, and τ) were estimated to find the common relaxation form, using an iterative approach based on the different relaxation models (Shen *et al.,* 1994). The power-law form gives a poor fit to the time series, and we omitted it. Figure 5 shows the best-fit logarithmic and exponential relaxation forms for one continuous site (UCGT, Fig. 5a) and one campaign site (SISL, Fig. 5b) as examples. Both functional forms provide a reasonable fit to the station time series. The logarithmic relaxation form (τ = 19 days) shows a marginally better fit to the time series for the first week or so following the earthquake, which shows highly accelerated strain. However, the best result is obtained by the exponential relaxation form (τ = 57 days) for the entire time period. The time series of station displacements are shown together with the best-fit exponential curves in Figure 3. The east components show most clearly the exponential relaxation behavior.

The amplitudes of the relaxation based on the exponential model are mapped in Figure 6. The amplitudes are relative to the regional continuous site MADT. To estimate the cumulative displacements for the 298 days, the estimated exponential relaxation model for each site is extrapolated to a common epoch (day 298). Uncertainties are also estimated using the uncertainty limits of the exponential relaxation model. The estimated cumulative displacements and their uncertainties are listed in Table 1. Figures 7A–C show cumulative site displacements for the 298- and 75-day postseismic time intervals and coseismic displacements relative to site MADT. The large uncertainty for the 298-day postearthquake cumulative displacements relative to those for the 75-day interval reflects uncertainties in the exponential model parameters.

Discussion

We interpret the accelerated strain during the early postseismic period to be due to continued faulting (afterslip) along the coseismic fault segments and in the lower crust (Reilinger *et al.,* 2000; Bürgmann *et al.,* 2001). This interpretation is supported by our analysis of the largest aftershock (13 September 1999, M_L 6.2, M_w 5.9). In this case, we were able to invert site displacements for the aftershock fault parameters. Although not tightly constrained by the displacement data, the aftershock involved right-lateral slip on a vertical fault plane located near the İzmit epicenter (Fig. 4), demonstrating that at least a part of the postearthquake site displacements reflect afterslip on the coseismic fault. However, total moment release in aftershocks is roughly an order of magnitude less than the postseismic geodetic moment (determined from models of afterslip for a 75-day period), indicating that most postearthquake deformation occurs aseismically (Reilinger *et al.,* 2000; Bürgmann *et al.,* 2001). On the other hand, the good exponential fit to the time series for the full 298 days suggests a component of viscoelastic deformation (Shen *et al.,* 1994; Savage and

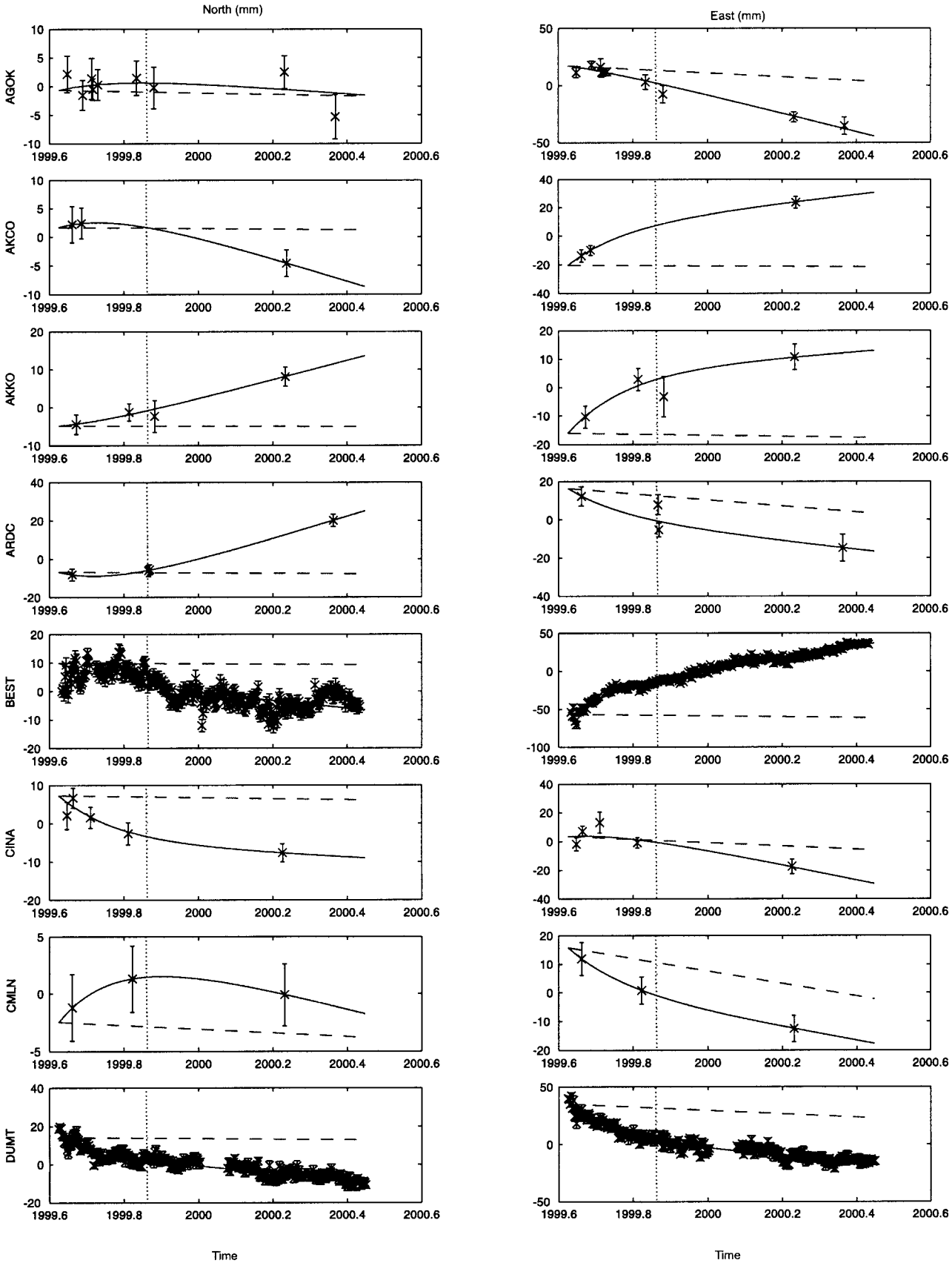

Figure 3. Time series of north and east coordinates for each site with the estimated exponential relaxation models with the common 57-day τ (solid line). Dashed lines show the estimated rate of change of site coordinates during the pre-earthquake period (Bürgmann *et al.*, 2001). The dotted vertical line indicates the time of the Düzce earthquake. The error bars of the daily solutions equal one standard deviation. Note different scales for site motions.

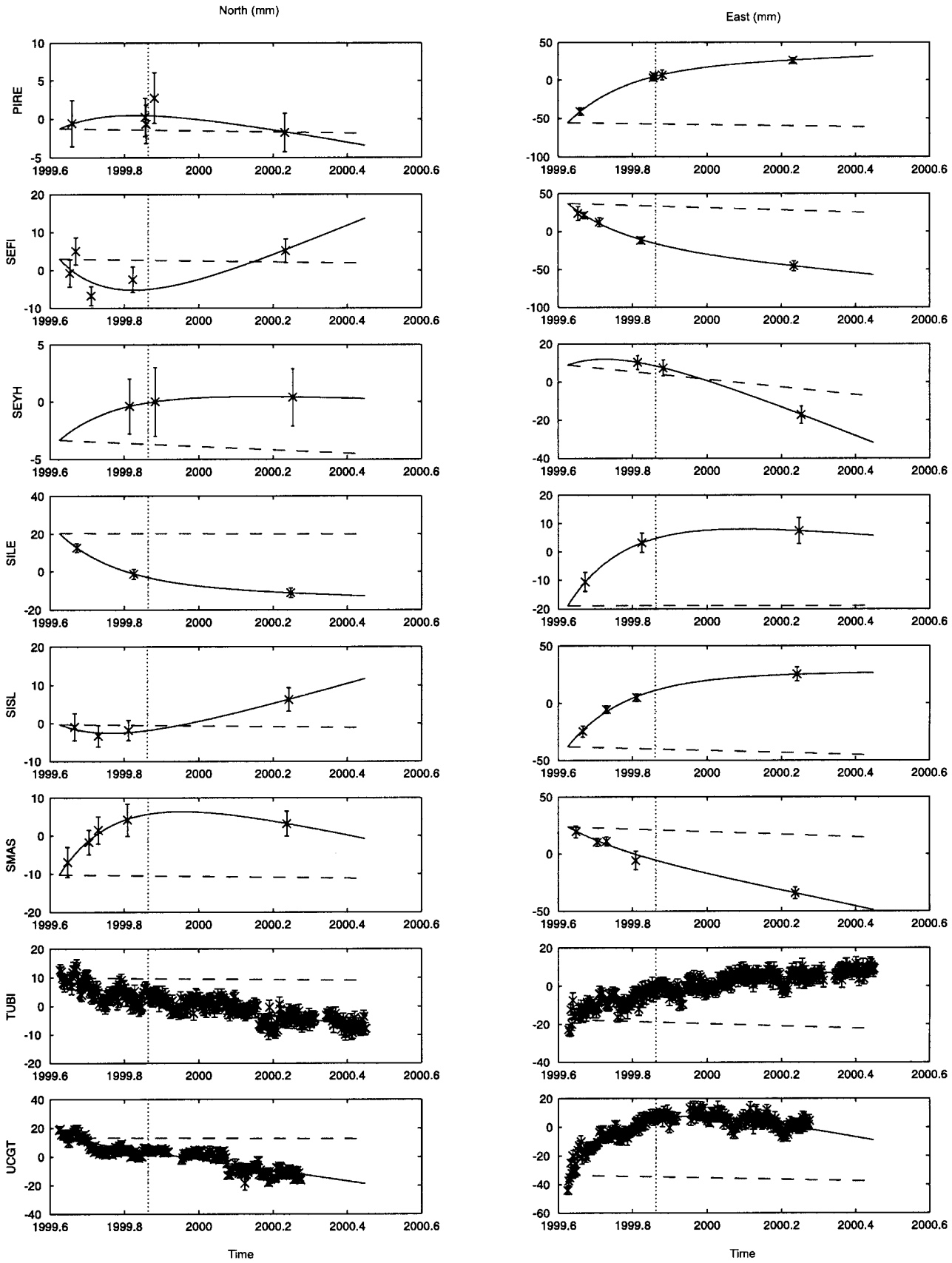

Figure 3. *(Continued).*

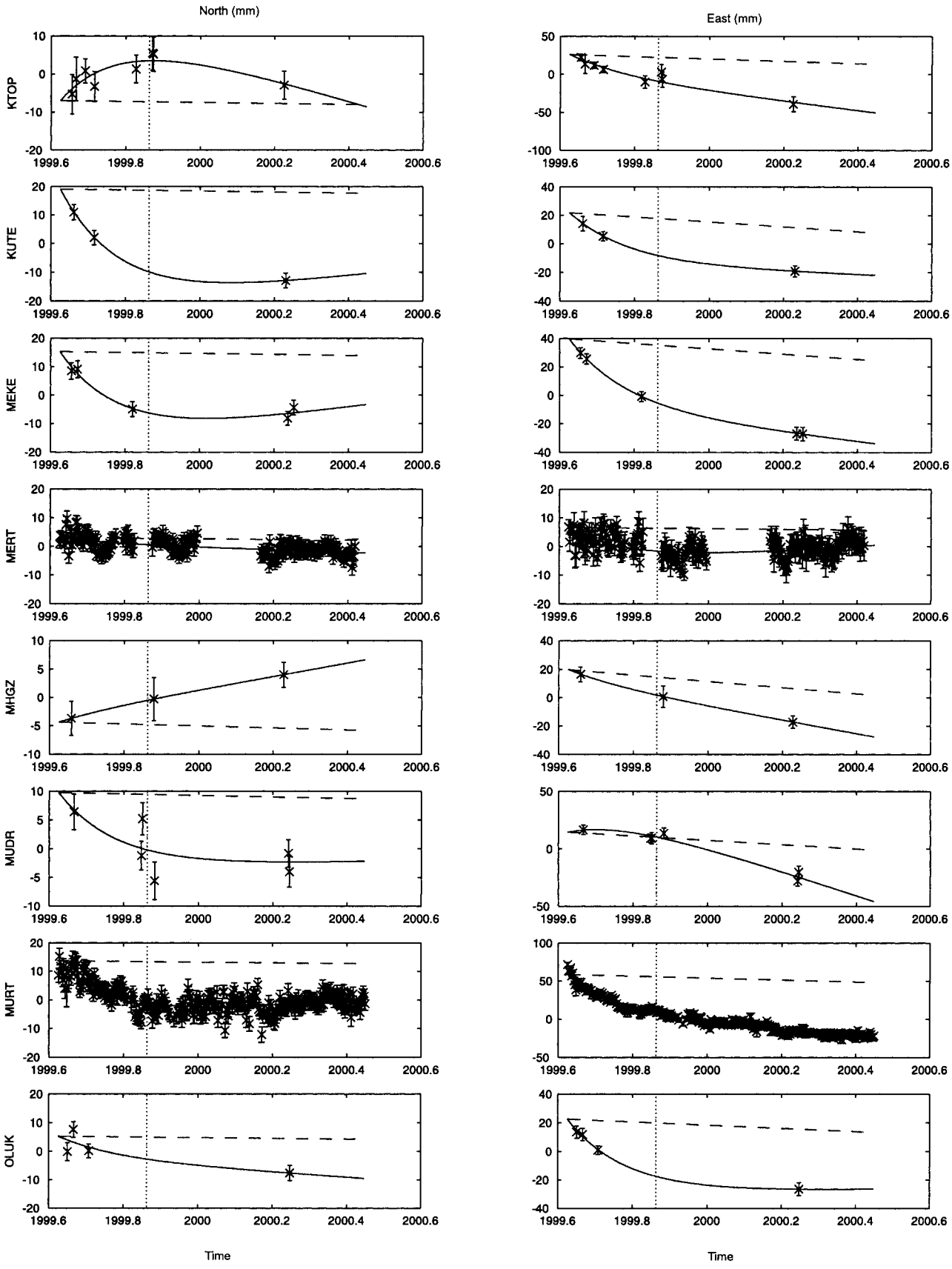

Figure 3. *(Continued).*

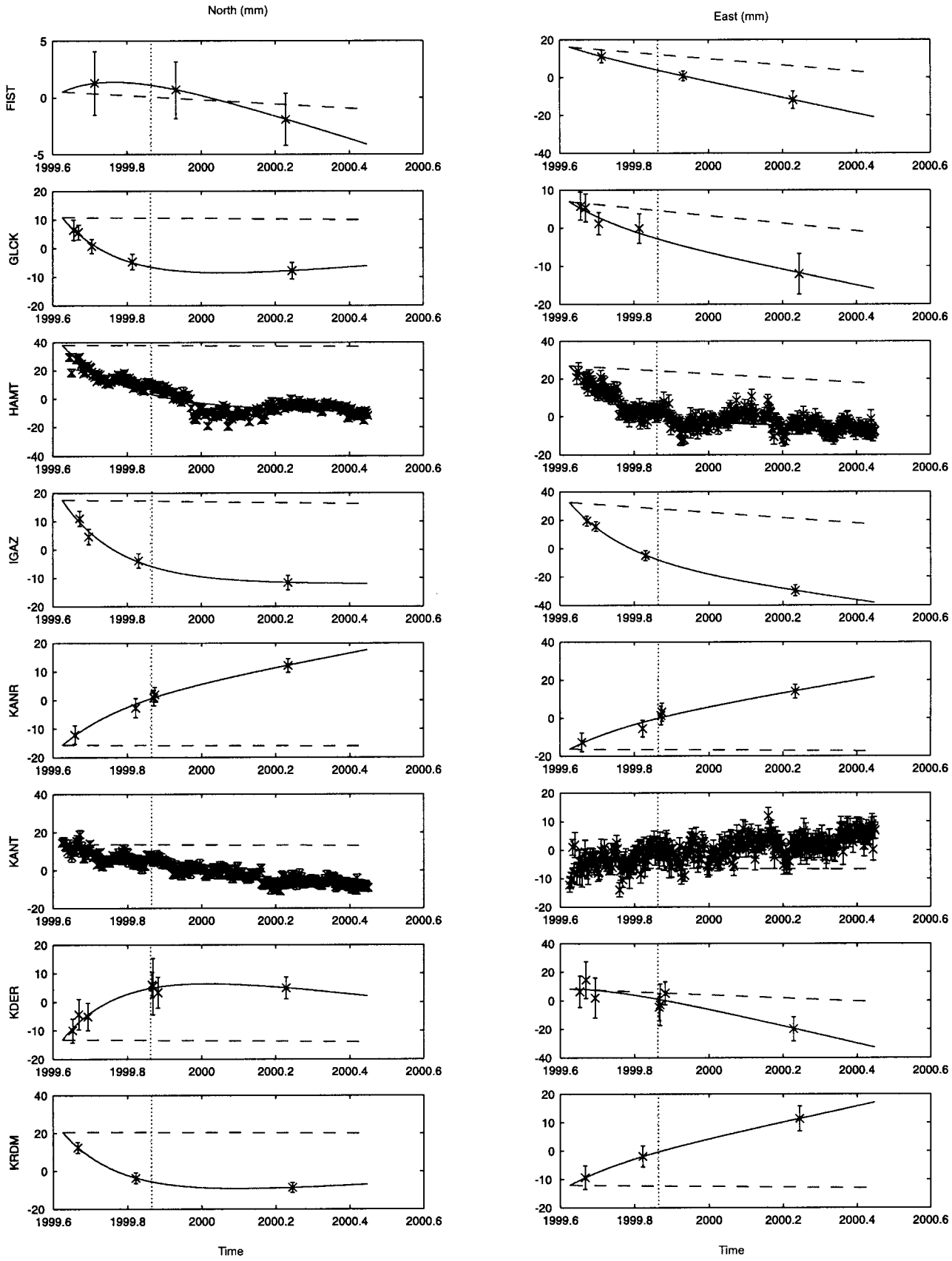

Figure 3. *(Continued).*

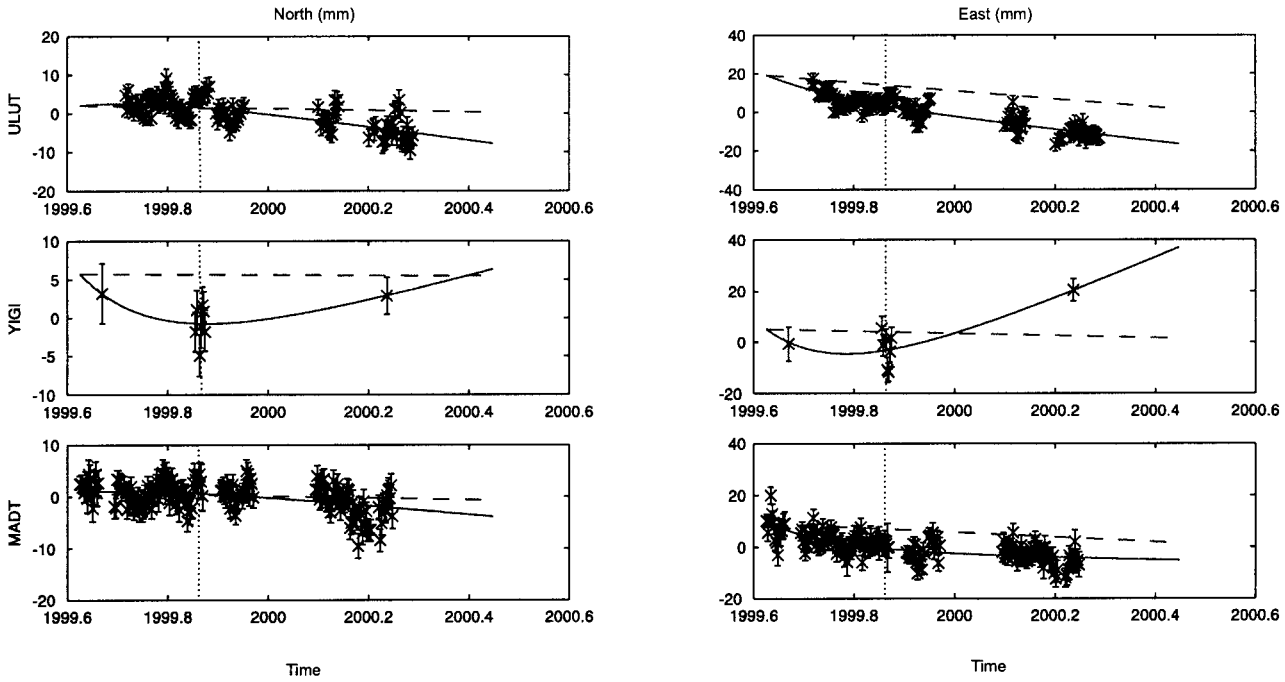

Figure 3. *(Continued).*

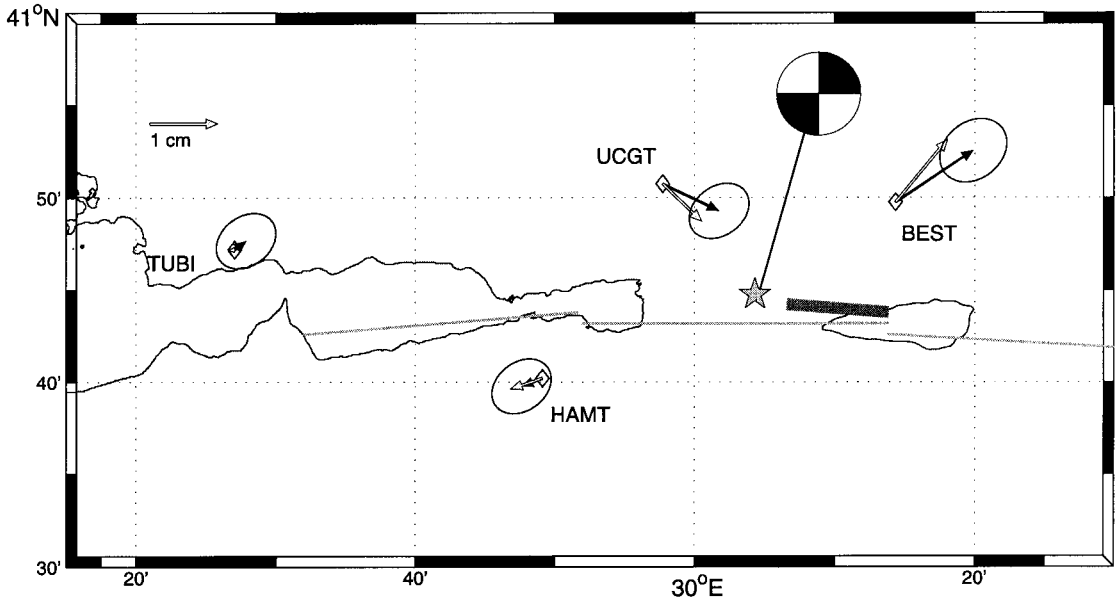

Figure 4. The modeling results of the biggest aftershock (13 October 1999, M_L 6.2, M_w 5.9). The black arrows with 95% confidence ellipses show the observations and the gray arrows show the model results. The thick short line indicates the surface projection of the modeled fault segment. The thin lines show the fault rupture of the main event (Reilinger *et al.,* 2000), and a star shows the seismically determined location of the event. Our model parameters: width, 10 km; depth to top of fault, 10 km; dip, 90°; estimated strike slip, -0.3693 ± 0.0176 m; geodetic moment magnitude, M_w 5.95. We also show the fault plane solution of the event (Özalaybey *et al.,* 2001).

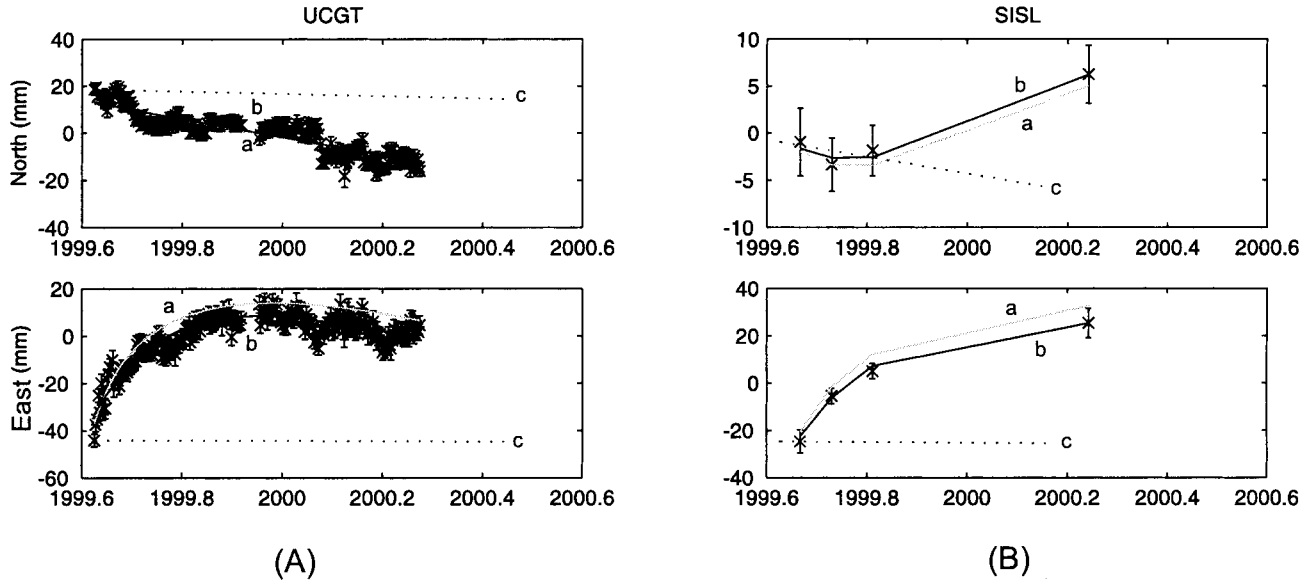

Figure 5. (A) Station displacements for the continuous UCGT station, and (B) for the campaign site SISL. The estimated logarithmic (a) and exponential (b) relaxation models, and the pre-earthquake steady state site motion (Bürgmann *et al.,* 2001) (c) for horizontal components are also shown.

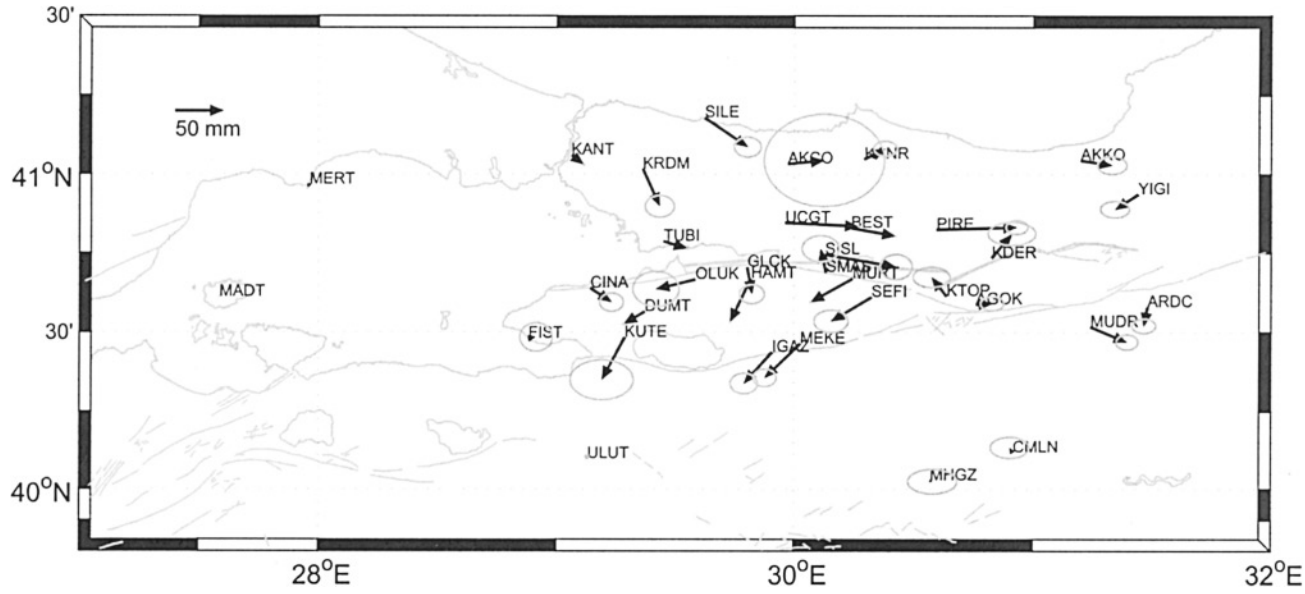

Figure 6. Relaxation amplitudes with 95% confidence ellipses estimated from the exponential relaxation model. Amplitudes are relative to station MADT.

Svarc, 1997), following the initial phase of rapid afterslip (Figs. 3 and 5).

To first-order, relaxation amplitudes (Fig. 6) and total station displacements (Fig. 7A and B) show little systematic variation as a function of distance from the coseismic fault out to distances of about 50–70 km (i.e., 3–5 fault depths) from the fault. This indicates that irrespective of the mechanism that is driving deformation (i.e., afterslip and/or viscoelastic relaxation) it is occurring relatively deep in the earth (i.e., below the seismogenic layer). This conclusion is supported by afterslip modeling studies that locate the largest afterslip at depths of 20–40 km (Reilinger *et al.,* 2000; Burgmann *et al.,* 2001).

Total station displacements (Fig. 7A) show the dominant fault-parallel motions in the near field. The deformation pattern is similar to the postseismic displacement results for the first 75 postseismic days (Fig. 7B). This similarity indicates that the model used to remove Düzce coseismic displacements was reasonably successful. On the other hand, the relatively large displacements of sites in the extreme

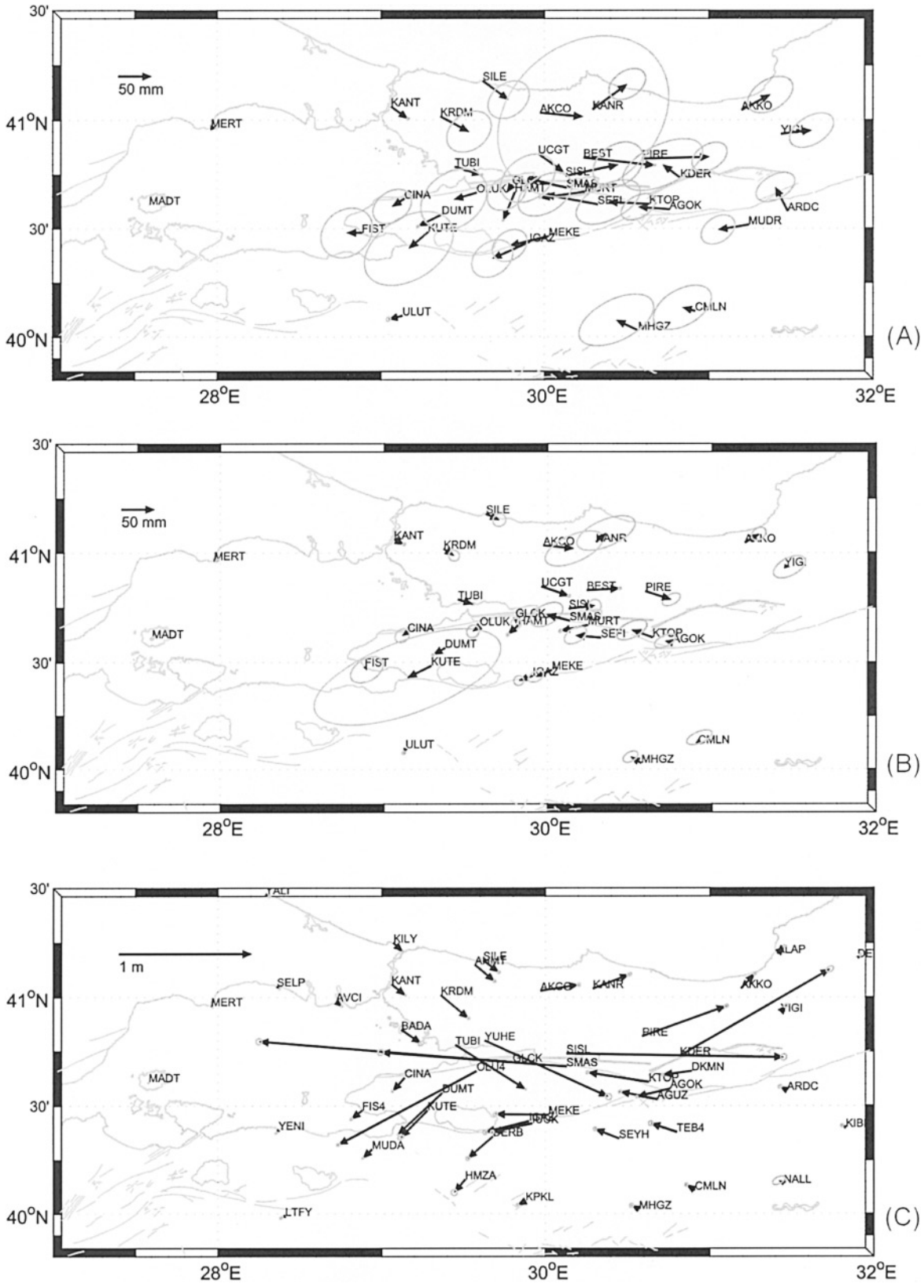

Figure 7. Total displacements for (A) the first 298 days following the Izmit earthquake and (B) the first 75 days following the earthquake. (C) Coseismic displacements. Uncertainties are 95% confidence ellipses. Displacements are relative to station MADT. (B) and (C) are modified from Reilinger *et al.* (2000).

eastern part of the network suggest that the Düzce coseismic model did not completely eliminate coseismic displacements, and/or that Düzce postseismic deformations influence these sites.

There appear to be some systematic differences between the patterns of coseismic and postseismic displacements (Fig. 7). Sites located adjacent to the central segment of the coseismic fault, particularly south of the fault (i.e., MEKE, IGAZ), show larger southerly components of motion during the postseismic period. In contrast, sites located adjacent to the eastern segment of the coseismic fault appear to be more fault-parallel than the coseismic displacements. This is best illustrated by site PIRE. In contrast, coseismic and postseismic displacements show similar patterns adjacent to the westernmost segment of the coseismic fault. These features persist in both the 75- and 298-day displacement fields, indicating that they do not result from the Düzce earthquake. There are a number of possible explanations for these observations, including sympathetic slip on secondary faults south of the coseismic fault (Wright *et al.,* 2001) influencing the coseismic displacements and spatial variations in crustal rheology. Alternatively, the different coseismic and postseismic patterns may reflect variations in the mechanisms of coseismic and postseismic deformation. In terms of models of afterslip, these differences suggest that postseismic afterslip extends east of the coseismic slip. In this case, sites that are adjacent to the central part of the coseismic fault are located in the western part of the postseismically slipping fault and thus display a larger fault normal component. Likewise, sites located adjacent to the east end of the coseismic fault are adjacent to the largest postseismic slip and thus show predominantly fault-parallel motion. On the other hand, the similarities in coseismic and postseismic deformation patterns adjacent to the western coseismic segment suggest that postseismic slip occurred on and below the segment that had the largest coseismic slip—that is, postseismic slip did not extend much west of the coseismic fault. These qualitative observations are borne out by detailed afterslip models, at least for the period leading up to the Düzce earthquake (Reilinger *et al.,* 2000; Burgmann *et al.,* 2001).

Conclusions

We report on the temporal and spatial character of postseismic deformation during the first 298 days following the İzmit earthquake using continuously recording and survey mode GPS sites distributed around the coseismic fault. The edited station displacements (i.e., after minimizing the effects of the Düzce earthquake, aftershocks, and removing daily outliers) can be fit by an exponentially decaying relaxation function with a 57-day relaxation time. Following a phase of rapid postseismic displacements, the postseismic motions appear consistent with a simple exponential stress relaxation model providing information about the mechanical behavior of the deep fault zone and the surrounding areas of the crust and upper mantle.

The close similarity between the 75- and 298-day postseismic deformation patterns suggests that the major coseismic motions of the Düzce earthquake were effectively removed from the time series of site motions. The postseismic station displacements show little dependence on distance from the coseismic fault out to distances exceeding 50 km, indicating that the processes giving rise to postearthquake deformation are predominantly occurring below the seismogenic layer (15–20 km).

We identify systematic differences between the patterns of coseismic and postseismic deformations adjacent to the central and eastern segments of the coseismic fault. With respect to the afterslip models of postseismic deformation, these differences suggest that afterslip was largest east and below the main coseismic slip region of the fault plane. In contrast, the similar coseismic and postseismic patterns on the west end of the coseismic fault argue against substantial afterslip west of the main coseismic slip segment. These qualitative conclusions are supported by detailed modeling studies (Reilinger *et al.,* 2000; Burgmann *et al.,* 2001). The propagation of afterslip east of the main coseismic fault slip region may have helped to trigger the Düzce earthquake (Hearn *et al.,* 2001). Because stress redistribution accompanying and following the earthquake will contribute to the stress loading of adjacent fault segments, postseismic relaxation, whether due to fault slip or viscoelastic relaxation, should be considered in seismic risk studies based on the Coulomb failure stress (e.g., Hubert-Ferrari *et al.,* 2000; Parsons *et al.,* 2000).

We require data over a much longer time span to adequately characterize all phases of the postseismic transients following the İzmit earthquake. However, based on the modeling results of Bürgmann *et al.* (2001) for the period between the İzmit and Düzce mainshocks (87 days) and our interpretation for the 298-day period following the İzmit earthquake, we can define a postearthquake behavior in which (1) rapid afterslip follows the sudden stress pulse from the mainshock, (2) more steady long-term deformation follows the early transient and appears to be due to processes primarily below the seismogenic layer, and (3) continuous loading at depth might contribute to accelerated viscous flow in the lower crust and loading of neighboring faults.

Acknowledgments

This research was supported in part by Boğaziçi University Research Fund Grant 01T302, the NSF grants EAR-9909730 and INT-9909619 to MIT, and a grant by the World Bank to TÜBİTAK, MRC. The authors thank Z. K. Shen for information about postseismic relaxation functions and two anonymous referees for helpful comments.

References

Ayhan, E., R. Bürgmann, S. McClusky, O. Lenk, B. Aktug, E. Herece, and R. E. Reilinger (2001). Kinematics of the M_w = 7.2, 12 November 1999, Düzce, Turkey Earthquake, *Geophys. Res. Lett.* **28,** no. 2, 367–370.

Barka, A. (1997). Neotectonics of the Marmara Sea region, in *Active Tectonics of Northwestern Anatolia: The Marmara Poly-Project,* C. Schindler and M. Pfister (Editors), ETH Zurich, Zurich, Switzerland, 55–87.

Bürgmann, R., S. Ergintav, P. Segall, L. Hearn, S. McClusky, R. E. Reilinger, H. Woith, and J. Zschau (2002). Time-dependent distribution afterslip on and deep below the İzmit earthquake rupture, *Bull. Seism. Soc. Am.* **92,** no. 1, 126–137.

Bürgmann, R., P. Segall, M. Lisowski, and J. Svarc (1997). Postseismic strain following the 1989 Loma Prieta earthquake from GPS and leveling measurements, *J. Geophys. Res.* **102,** 4933–4955.

Chen, W. P., and P. Molnar (1983). Focal depths of intracontinental and intraplate earthquakes and their implication for the thermal and mechanical properties of the lithosphere, *J. Geophys. Res.* **88,** 4183–4214.

Hearn, E. H., R. Bürgmann, and R. E. Reilinger (2002). Dynamics of İzmit postseismic deformation and loading of the Düzce earthquake hypocenter, *Bull. Seism. Soc. Am.* **92,** no. 1, 172–193.

Herring, T. A. (2000). *GLOBK: Global Kalman Filter VLBI and GPS Analysis Program Version 10.0,* Massachusetts Institute of Technology, Cambridge, Massachusetts.

Hubert-Ferrari, A., A. Barka, E. Jacques, S. S. Nalbant, B. Meyer, R. Armijo, P. Tapponnier, and G. C. P. King (2000). Seismic hazard in the Marmara Sea region following the 17 August 1999 İzmit earthquake, *Nature* **404,** 269–272.

King, R. W., and Y. Bock (1998). *Documentation for the GAMIT Analysis Software, Release 9.7,* Massachusetts Institute of Technology, Massachusetts, Cambridge.

Marone, C., C. H. Scholtz, and R. Bilham (1991). On the mechanics of earthquake afterslip, *J. Geophys. Res.* **96(B5),** 8441–8452.

McClusky S., S. Balssanian, A. Barka, C. Demir, S. Ergintav, I. Georgiev, O. Gurkan, M. Hamburger, K. Hurst, H. Kahle, *et al.* (2000). Global Positioning System constraints on plate kinematics and dynamics in the eastern Mediterranean and Caucasus, *J. Geophys. Res.* **105,** 5695–5719.

Okada, Y. (1985). Surface deformations due to shear and tensile faults in a half space, *Bull. Seism. Soc. Am.* **75,** 1135–1154.

Özalaybey, S., M. Ergin, M. Aktar, C. Tapırdamaz, F. Biçmen, A. Yörük (2002). The 1999 İzmit earthquake sequence in Turkey: seismological and tectonic aspects, *Bull. Seism. Soc. Am.* **92,** no. 1, 376–386.

Parsons, T., S. Toda, R. S. Stein, A. Barka, and J. H. Dieterich (2000). Heightened odds of large earthquakes near Istanbul: an interaction-based probability calculation, *Science* **288,** 661–665.

Pollitz, F. F., R. Bürgmann, and P. Segall (1998). Joint estimation of afterslip rate and postseismic relaxation following the 1989 Loma Prieta earthquake, *J. Geophys. Res.* **103,** 26,975–26,992.

Ranalli, G. (1987). *Rheology of the Earth,* Allen & Unwin Inc., Winchester, Massachusetts.

Reilinger, R. E., S. McClusky, R. Bürgmann, S. Ergintav, A. Barka, H. Meteris, O. Gurkan, K. L. Feigl, N. Yalçın, and M. N. Toksöz (2000). Coseismic and postseismic fault slip for the 17 August 1999, M = 7.5, İzmit, Turkey earthquake, *Science* **289,** 1519–1524.

Savage, J. C. (1980). Dislocation in seismology, in *Dislocation in Solids,* Vol. 3, F. R. N. Nabarro (Editor), North-Holland, Amsterdam, 251–339.

Savage, J. C. (1990). Equivalent strike-slip earthquake cycles in half-space and lithosphere–asthenosphere Earth models, *J. Geophys. Res.* **95,** 4873–4879.

Savage, J. C., and W. H. Prescott (1978). Asthenospheric readjustment and the earthquake cycle, *J. Geophys. Res.* **83,** 3369–3376.

Savage, J. C., and J. L. Svarc (1997). Postseismic deformation associated with the 1992 M_w = 7.3 Landers earthquake, southern California, *J. Geophys. Res.* **102,** 7565–7577.

Scholz, C. H. (1988). The critical slip distance for seismic faulting, *Nature* **336,** 761–763.

Shen, Z. K., D. D. Jackson, Y. Feng, M. Cline, M. Kim, P. Fang, and Y. Bock (1994). Postseismic deformation following the Landers earthquake, California, 28 June 1992, *Bull. Seism. Soc. Am.* **84,** 780–791.

Thatcher, W. (1983). Nonlinear strain buildup and the earthquake cycle on the San Andreas fault, *J. Geophys. Res.* **88,** 5893–5902.

Toksöz, M. N., A. F. Shakal, and A. J. Michael (1979). Space–time migration of earthquakes along the North Anatolian fault zone and seismic gaps, *Pageoph* **117,** 1258–1270.

Tse, S. T., and J. R. Rice (1986). Crustal earthquake instability in relation to the depth variation of frictional slip properties, *J. Geophys. Res.* **91,** 9452–9472.

Wright, T. J., E. J. Fielding, and B. E. Parsons (2001). Triggered slip: observations of the 17 August 1999 İzmit (Turkey) earthquake using radar interferometry, *Geopyhys. Res. Lett.* **25,** no. 6, 1079–1083.

Yalçin, N., S. Ergintav, M. Aktar, C. Gurbuz, O. Gurkan, H. Eyidogan, A. Barka, E. Ayhan, O. Lenk, R. Reilinger, and N. Toksöz (1999). Seismic hazard assessment in the Marmara Sea Region, International Union of Geodesy and Geophysics (IUGG99), 18–30 July, Birmingham, United Kingdom.

The Scientific and Technical Research Council of Turkey (TÜBİTAK)
MRC, Earth and Marine Sciences Research Institute
Gebze 41470
Turkey
semih.Ergintav@posta.mam.gov.tr
(E.S., R.Ç., A.B.)

Department of Earth and Planetary Science
301 McCone Hall
University of California, Berkeley
Berkeley, California 94720
(R.B.)

Department of Earth, Atmospheric, and Planetary Sciences
Massachusetts Institute of Technology
Cambridge, Massachusetts 02142
(S.M., R.E.R.)

General Command of Mapping
Cebeci
Ankara, Turkey
(O.L.)

Istanbul Technical University
Eurasia Earth Science Institute
Ayazağa
Istanbul, Turkey
(A.B.)

Kandilli Observatory and Earthquake Research Institute
Boğaziçi University
Istanbul, Turkey
(H.Ö.)

Manuscript received 22 September 2000.